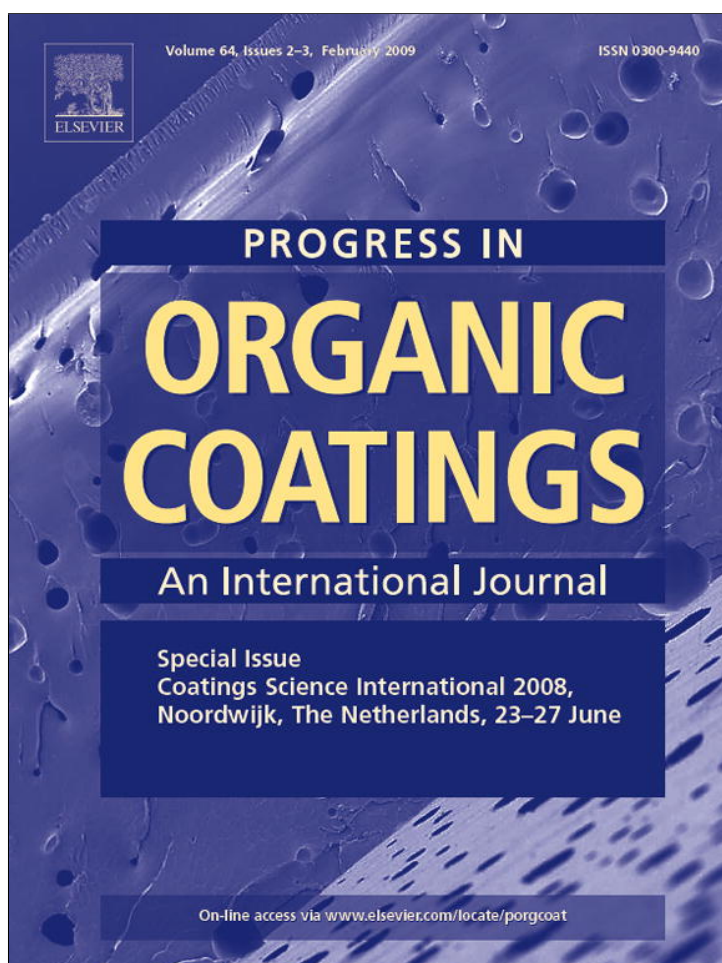


Provided for non-commercial research and education use.  
Not for reproduction, distribution or commercial use.



This article appeared in a journal published by Elsevier. The attached copy is furnished to the author for internal non-commercial research and education use, including for instruction at the authors institution and sharing with colleagues.

Other uses, including reproduction and distribution, or selling or licensing copies, or posting to personal, institutional or third party websites are prohibited.

In most cases authors are permitted to post their version of the article (e.g. in Word or Tex form) to their personal website or institutional repository. Authors requiring further information regarding Elsevier's archiving and manuscript policies are encouraged to visit:

<http://www.elsevier.com/copyright>



Contents lists available at ScienceDirect

## Progress in Organic Coatings

journal homepage: [www.elsevier.com/locate/porgcoat](http://www.elsevier.com/locate/porgcoat)

## Radiation curing technology: An attractive technology for metal coating

P. Roose<sup>a,\*</sup>, I. Fallais<sup>a</sup>, C. Vandermiers<sup>b</sup>, M.-G. Olivier<sup>b</sup>, M. Poelman<sup>c</sup><sup>a</sup> Cytec Surface Specialties, Anderlechtstraat 33, B-1602 Drogenbos, Belgium<sup>b</sup> Faculté Polytechnique Mons, Rue de l'Épargne 56, B-7000 Mons, Belgium<sup>c</sup> Materia Nova, Rue de l'Épargne 56, B-7000 Mons, Belgium

## ARTICLE INFO

## Article history:

Received 5 June 2008

Received in revised form 14 July 2008

Accepted 13 August 2008

## Keywords:

Radiation curing

UV-coating

Metal

Adhesion

Shrinkage

Electrochemical impedance spectroscopy (EIS)

Barrier properties

## ABSTRACT

The introduction of new tailor-made (meth)acrylated oligomers has extended the potential use of the radiation curing technology to metal coating applications where adhesion, flexibility and corrosion resistance are of prime importance. In this paper, we discuss the properties of three fairly simple clearcoat systems spanning a range of glass transition temperatures between  $\approx 10$  and  $70$  °C. The systems were obtained by combination of two original urethane acrylate resins and two reactive diluents.

Practical performance tests typically used to establish coating profiles in the metal industry (i.e., mechanical testing, adhesion, salt-spray test, etc.) were performed on ultraviolet (UV)-coated galvanised steel. In addition, the barrier properties of coated steel panels were systematically investigated at different coating thicknesses using electrochemical impedance spectroscopy. These results are analysed in terms of relevant physico-chemical characteristics such as conversion, volume contraction, swelling, viscoelastic and tensile behaviour determined on free-standing coating layers of the three formulations.

© 2008 Elsevier B.V. All rights reserved.

## 1. Introduction

Since the early seventies, the radiation curable coatings technology has gained full acceptance in a number of industrial applications like wood coating or printing inks and varnishes. The major driving forces behind this technology, as compared to conventional ones, are (i) high productivity due to the fast polymerization rates, (ii) excellent surface properties, (iii) low floor space requirement, and (iv) significant environmental benefits due to the energy-efficiency of the process and the use of solvent-free resins complying with the stringent legislation [1].

These advantages are also very attractive for metal coating applications. In this growing and challenging application area, three segments can be identified, i.e., (i) coil coatings for the building, automotive and domestic appliance sectors, (ii) packaging coatings for cans, easy opening parts, twist-off, etc., and (iii) coatings for the general industry such as the pipes and tubes industry, earth moving machines and three-dimensional pieces like valves, breaks, etc.

Even if an increasing success is noticed, the growth potential for the radiation curing technology in metal coating is still important. The product requirements for metal coatings are particularly

demanding. In addition to the excellent surface performances, adhesion to various metal substrates (e.g., aluminum, steel, tin plated steel), flexibility and corrosion protection of the coated metal are of paramount importance [2].

In many applications the coated or prepainted metal undergoes further deformation or moulding treatments. Hence, the optimization of the flexibility and especially the adhesion of the coating system require particular attention. Typical ultraviolet (UV)-curable formulations consist of (meth)acrylated oligomers and reactive diluents blended with additives which upon curing form a highly crosslinked coating layer. The high crosslink density often leads to hard materials with limited flexibility and poor adhesion to the metal substrate. In the quest for solutions, one is often bound by the molecular weight of the resin which should be low enough to achieve a reasonable viscosity, while still keeping the crosslink density sufficiently low in order to reach the required flexibility for the cured coating.

This study focuses on the performances reached with two original urethane acrylates developed with the aim of meeting these stringent requirements. They are studied in three fairly simple clearcoat systems spanning a range of glass transition temperatures between  $\approx 10$  and  $70$  °C.

Practical performance tests typical for the metal industry (i.e., mechanical testing, adhesion, salt-spray test, etc.) are performed on UV-coated galvanised steel. In addition, the barrier properties of coatings are systematically investigated at different coating thick-

\* Corresponding author at: Research and Development, Cytec Surface Specialties, Anderlechtstraat 33, B-1620 Drogenbos, Belgium. Tel.: +32 2 334 57 54.

E-mail address: [patrice.roose@cytec.com](mailto:patrice.roose@cytec.com) (P. Roose).

**Table 1**  
Description of the oligomer resin and the reactive diluent used in the formulations of the L, M and H clearcoat systems. The viscosity of the formulation is also provided.

Formulation	Oligomer resin		Reactive diluent		Viscosity (Pa s)
L	UA1	Polyester urethaneacrylate	Ebecryl™ 114	Ethoxylated phenol acrylate ( $f=1$ )	9.8
M	UA2	Unsaturated polyester urethaneacrylate	Ebecryl™ 114	Ethoxylated phenol acrylate ( $f=1$ )	5.3
H	UA2	Unsaturated polyester urethaneacrylate	Ebecryl™ OTA480	Propoxylated glycerol triacrylate ( $f=3$ )	12.5

nesses using electrochemical impedance spectroscopy (EIS) [3–7]. These results are analysed in terms of relevant physico-chemical characteristics such as conversion, volume contraction, swelling, viscoelastic and tensile behaviour determined on free-standing coating layers of the three formulations.

## 2. Materials and methods

### 2.1. Sample preparation

#### 2.1.1. Liquid resin formulations

Two newly developed urethane acrylate oligomers were selected for this study. Both have been designed to meet the stringent product profile of metal coating.

UA1 is a polyester urethane acrylate derived from a hydroxyl-terminated polyester, a polyfunctional isocyanate and an olefinically unsaturated monomer containing hydroxyl groups. The polyester is typically based on a linear saturated dicarboxylic acid having from 4 to 14 carbon atoms and a branched chain aliphatic diol (e.g., propylene glycol, neopentyl glycol, 1,3-propanediol). It was found that this kind of composition provides good surface properties along with improved adhesion, flexibility and corrosion resistance making it suitable for application on metal.

UA2 is an unsaturated polyester urethane acrylate derived from an unsaturated hydroxyl-terminated polyester, a polyfunctional isocyanate and an olefinically unsaturated monomer containing hydroxyl groups. It was found that the incorporation of unsaturated fatty acids in polyester urethane acrylates reduces their viscosity and markedly improves the adhesion on metal.

Prior to formulation, the oligomers were diluted with a reactive diluent in a fixed oligomer-to-diluent ratio of 70:30 wt%. A mono- and a trifunctional acrylate compound were used as diluent (cf. Table 1). Simple clearcoat formulations were then prepared using a standard package of additives in order to emphasize the contribution of the oligomer resin and the diluent on the coatings performances. In addition to the photoinitiators (3 wt% Additol™ CPK<sup>1</sup> and 2 wt% Additol™ TPO<sup>2</sup>), a metal adhesion promoter (5 wt% Ebecryl™ 171) and levelling agents (1 wt% Additol™ VXL4930 and 0.4 wt% BYK346) were used to obtain ready-to-use formulations. All materials were provided by Cytec Surface Specialties except BYK 346 (BYK).

The three formulations described in Table 1 lead to coatings characterized by a low (15 °C), medium (34 °C) and high (66 °C) glass transition temperature ( $T_g$ ) and are respectively referred to as L, M and H throughout the text.

#### 2.1.2. Free-standing coating films

The physico-chemical characteristics of the solid coatings were determined using free standing films. The films were prepared on a glass substrate cleaned with acetone and isopropanol prior to use. The liquid formulation was applied on the substrate with a bar coater. Depending on the formulation viscosity, the bar coater was chosen by trial and error to get a free film with a thickness

close to 100  $\mu\text{m}$ . The films were cured using a 120 W  $\text{cm}^{-1}$  non-focalized medium pressure mercury vapour lamp at a belt speed of 5  $\text{m min}^{-1}$ . The number of passes under the lamp was adjusted for each formulation in order to have a minimum conversion of 90% for the acrylate double bonds. After curing, the film was removed from the glass substrate with a cutter.

#### 2.1.3. Coated steel panels

Coated steel panels were prepared for the EIS measurements and the application tests using hot dip galvanized steel panels without pretreatment (Senzimirverzinkte Stahlbleche Gardobond E HDG, supplied by Chemetall). The panels were conditioned as follows. The protecting oil was first removed with a tissue. Next, the panel was immersed for 10 s in a Gardoclean S 5163 bath (Chemetall), rinsed with tap water and immersed in a demineralised water bath for 5 min. Finally, the panels were dried with a hair dryer.

One or multiple layers of tape (Tesa AG 4104) were fixed on the sides of the panel to control the coating thickness. The liquid formulation was applied with a 2  $\mu\text{m}$  bar coater using the tape as an application guide. The curing conditions were similar as for the free films (cf. Section 2.1.2). The number of passes under the lamp was adjusted for each formulation to have a good curing. This is commonly assessed by empirical tests such as thumb twist, talc reactivity and fingernail scratch. The experience showed that after five passes at 5  $\text{m min}^{-1}$  the double bonds conversion was always at least 90% (cf. Section 2.3.1). Depending on the  $T_g$  however, coatings may remain tacky at high conversion and the empirical tests fail to assess the degree of curing.

The coating thickness was measured using a Heidenhain MT-25B length gauge, a minimum of six measurements was performed for each panel. Table 2 illustrates the variance of the coating thickness for different panel at a target value of 20  $\mu\text{m}$ . For convenience, the samples are identified using the target thickness.

### 2.2. Application tests

The coated steel panels were tested for solvent resistance (ECCA T11 test method), cross-hatch adhesion (ISO 2409), adhesion and resistance to cracking on bending (T-bend test EN 13523-7), adhesion and resistance to cracking on rapid deformation (reverse impact test ISO/DIS 6272—ASTM D 2794), adhesion on slow drawn deformation (Cupping test (Erichsen) ISO 1520) and salt spray cabinet test (ASTM B117-85). It is noted that in all the deformation tests, the constraint was applied on the backside of the panel (uncoated side).

**Table 2**  
Average coatings thicknesses for the L, M and H formulations at a target thickness of 20  $\mu\text{m}$ .

	L20	M20	H20
Average thickness and standard deviation ( $\mu\text{m}$ )	26.3 $\pm$ 1.5	25.9 $\pm$ 1.3	27.7 $\pm$ 3.1
	25.3 $\pm$ 1.2	28.9 $\pm$ 1.4	28.9 $\pm$ 2.1
	20.5 $\pm$ 1.7	20.7 $\pm$ 1.9	27.4 $\pm$ 2.9
	24.5 $\pm$ 2.5		
	22.3 $\pm$ 1.7		

<sup>1</sup> 1-Hydroxycyclohexyl phenyl ketone.

<sup>2</sup> 2,4,6-Trimethylbenzoyldiphenylphosphine oxide.

### 2.3. Physico-chemical characterization

#### 2.3.1. Double bond content and conversion after ultraviolet radiation-curing

The molar concentration of (meth)acrylic double bonds,  $N_{db}$ , in the liquid formulations was determined by high-resolution  $^1\text{H}$  NMR spectroscopy (Bruker Advance DPX300). A known amount of 1,3,5 bromobenzene was used as internal standard for quantification.

For the cured free-standing films, the conversion of the acrylic double bonds was determined by attenuated total reflection Fourier-transform infrared (ATR-FTIR) spectroscopy. The IR-spectra were collected using a PerkinElmer Spectrum 2000 FTIR Spectrometer equipped with a golden gate high-pressure micro-ATR accessory. With this ATR device, the active sampling area of the diamond crystal is about  $1.5\text{ mm}^2$ . The liquid samples were simply deposited with a pipette onto the ATR surface prior to analysis. In contrast, the solid film samples were applied under pressure to the flat surface of the diamond crystal in order to obtain a good contact. The change of absorbance at  $810\text{ cm}^{-1}$ ,  $A_{810}$ , between the liquid and the film is reported as (meth)acrylic double bond conversion, i.e.,  $(1 - A_{810\text{ film}}/A_{810\text{ liquid}})$ . Owing to the limited penetration depth of a few microns in ATR, the IR-absorption merely reflects the conversion at the surface of the film. To assess the curing homogeneity, conversion was measured at both sides of the film but no significant differences could be observed within experimental accuracy.

#### 2.3.2. Volume contraction

The volume contraction due to curing (often referred to as curing shrinkage) was estimated from the density change between the liquid and the cured solid state and is returned as  $(\rho_{\ell}/\rho_s - 1)$ . The liquid density,  $\rho_{\ell}$ , was measured using a calibrated pycnometer. The density of the cured coating,  $\rho_s$ , was determined by immersion of a circular piece of free-standing film in a gradient density column (Davenport Instruments). The density column was prepared using carefully degassed solutions of sodium bromide. The column was calibrated in the range 1.10–1.25 using standard marker floats. The position of the samples suspended in the column was recorded after 2 h and controlled after 24 h. Deviations were generally within experimental accuracy. Occasionally, an apparent density drift was noticed after 24 h due to the adsorption of air bubbles on the sample surface. All density measurements were conducted at  $23.0 \pm 0.5\text{ }^\circ\text{C}$ .

#### 2.3.3. Viscoelastic and tensile properties

The small-strain viscoelastic properties of the free-standing films were measured by dynamic mechanical analysis using a DMA 2980 of TA Instruments. Rectangular pieces ( $\approx 8\text{ mm} \times 12\text{ mm}$ ) of film were clamped vertically in the sample holder for tensile operation. The frequency of the sinusoidal strain deformation was 1 Hz and the amplitude was typically between 0.3 and 1%. The heating rate was  $3\text{ K min}^{-1}$ . The temperature at the maximum of the loss tangent peak was used to establish the glass transition temperature ( $T_g$ ). The width of the transition,  $\Delta T_g$ , is determined as the full-width at half maximum of the loss tangent peak. The plateau storage modulus,  $E'_0$ , is returned at a temperature  $T = T_g + 100\text{ }^\circ\text{C}$  beyond the glass transition.

The uniaxial stress-strain properties were measured at room temperature with a Zwick Z010 elongation testing machine at a cross-head speed of  $50\text{ mm min}^{-1}$ . Rectangular-shaped specimens of  $3\text{ cm} \times 1\text{ cm}$  were cut from the free-standing coating films for the tests. At least three independent measurements were performed for each film.

#### 2.3.4. Solvent swelling

Solvent swelling was estimated following an optical microscopy method. A square sample of the film ( $\approx 2\text{ mm} \times 2\text{ mm}$ ) was sand-

wiched between a microscope and a glass cover slide. The initial lengths of the sample diagonals ( $d_i$ ) were then captured from a magnified image obtained in transmission mode. Then, solvent (methylethylketone, MEK) was added at the borders of the glass assembly and, by capillary action, the sample was progressively soaked with the solvent. Upon addition of solvent, no significant increase in sample size was noticed after nearly 10 min and the final diagonal dimensions ( $d_f$ ) were again measured. The swelling factor is expressed as  $SF_{\text{MEK}} = d_f/d_i - 1$ .

#### 2.3.5. Contact angle and surface free energy

The surface free energies of the three coating systems were estimated from contact angle measurements using reference liquids of known surface tension. Flat UV-cured coatings were prepared by curing the liquid resin between two microscope glass slides separated by thin spacers. At least one glass surface was treated with a silane agent in order to help coating release from the glass prior to the contact angle measurements. Due to the affinity of the coating for some solvents and the wetting behaviour of the surface, most of the common reference liquids were not suitable for contact angle measurements. Distilled deionized water, however, provided stable axisymmetric droplets. The advancing contact angle was recorded using an OCA20 instrument of DataPhysics. A similar approach was followed for a cleaned HDG panel. In this case, we obtained reliable contact angle data with diiodomethane. With a single contact angle value at hand, we used the equation-of-state approach of Neumann et al. to estimate the surface free energy [8,9].

### 2.4. Electrochemical impedance spectroscopy

The electrochemical measurements were carried out at room temperature using a conventional three-electrode cell filled with the electrolytic solution (NaCl, 0.1 M). The working electrode was the coated metal sample with an exposed area of  $7\text{ cm}^2$ . The counter electrode was a platinum plate and all potentials were measured with respect to an Ag/AgCl reference electrode. The electrochemical cell was put in a Faraday cage in order to minimize external interference on the system.

The impedance measurements were performed over frequencies ranging from 100 kHz to 10 mHz using a 20 mV amplitude signal voltage. The spectra were acquired using a computer-controlled PARSTAT 2273 from Ametek.

The measurements were performed after different exposure times (i.e., 1, 3 and 7 days) in the electrolytic solution. During the first day, the impedance data were collected every 2 h in order to evaluate the water uptake occurring at short immersion times. All the measurements were repeated on three different samples to check reproducibility.

The film thickness of the exposed area was measured with a Minitest 3001 thickness gauge. The measurements were repeated three times on five different points. The reported thickness corresponds to the average of these data.

## 3. Results and discussion

### 3.1. Application performances for UV-coated galvanised steel

In practice, it is not unusual to find formulations of reactive acrylate resins where five to ten, or even more, different compounds are blended together. If one takes into account the complexity of the composition and the multiplicity of curing conditions, it is not surprising that the development of new UV-coatings refers to empirical methods and know-how. However, the clearcoat compositions considered in this work are fairly simple. Table 1 shows

**Table 3**

Results of solvent resistance, cross-hatch adhesion, Erichsen, T-bend, impact and salt-spray tests for coated galvanised steel at two thicknesses.

Coating	Solvent resistance (MEK DR) <sup>a</sup>	Cross-hatch	Erichsen (mm)	T-bend		Impact (J)		Salt spray <sup>b</sup>
				Cracks	adh	Cracks	adh	
L20	>100	0	>8	0	0.5	>18	>18	1
L100	>100	1	>8	0	0.5	>18	>18	/
M20	>100	0	>8	0	1	>18	>18	2
M100	>100	0	>8	0.5	1	>18	>18	/
H20	>100	0	>8	0.5	>1	2	15	3
H100	>100	2	6	>1	>1	2	<2	/

<sup>a</sup> MEK DR = methyl ethyl ketone double rubs.<sup>b</sup> Salt spray results are expressed using a comparative scale: 1 is the best corrosion protection resin, 3 is the worst one.

that 90 wt% of the bulk composition consists of a urethane acrylate oligomer and a reactive diluent whereas the remaining 10 wt% represents a mix of additives which is held constant.

Coating profiles for the metal industry are established from practical performance tests. In Table 3, the results are summarized for the three clearcoat formulations applied on zinc galvanised steel at two thicknesses. After UV-curing, contrasting coating properties were obtained. Most strikingly are the poor mechanical performances of the H-system where T-bend and impact tests are particularly unacceptable. In this kind of bending tests, the coating undergoes a tensile loading when the coated surface of the test panel is directed outwards. The tests provide an assessment of the fracture toughness of a coating. Failure can occur in the coating layer (cohesive) or at the interface with the substrate (adhesive) and is qualitatively reported by the “cracks” and “adh” levels [10]. The H-coating system also showed rapid degradation (edge corrosion and blistering) in the salt-spray climate chamber and is ranked far behind the other two systems. The L and M coating systems, prepared with the same reactive diluent (Ebecryl™ 114), exhibit properties that are much less departing. Overall, the L clearcoat reveals the best performances with better T-bend and salt-spray resistance as compared to the M-system. Obviously, the nature of the clearcoat dominates the performances but an effect of coating thickness is observed as well. In particular, adhesion decreases with increasing layer thickness. This behaviour has been reported previously and is related to an increase of the internal strain energy stored in the coating [11].

### 3.2. Physico-chemical properties of the free-standing UV clearcoats

The material properties of a radiation-cured coating are determined by the chemical composition and the structure. A detailed analysis of the structure is not a straightforward task, especially when complex compositions are involved. Few studies reported in the literature have attempted to unravel the structural and morphological details of model systems using localized analytical techniques [12]. Alternatively, bulk physical properties provide useful data that can be related to the material performance. To a certain extent, they also reveal features of the materials structure. For this purpose, we have prepared free-standing coating films of the three formulations L, M and H in the thickness range 80–120 μm. As mentioned before, the curing conditions were adjusted in order to reach a conversion of at least 90% for the (meth)acrylic double bonds. No significant deviation was found between the conversion of the two film sides and the average conversion rates are reported in Table 4. The  $T_g$  values of the UV-cured resins are 15, 34 and 66 °C, respectively. Noteworthy is the increasing width of the glass transition,  $\Delta T_g$ , upon increase of the  $T_g$  value. Actually, the onset of the glass transition is well below room temperature for the three coatings. A large glass transition is reminiscent of a broad relaxation spectrum

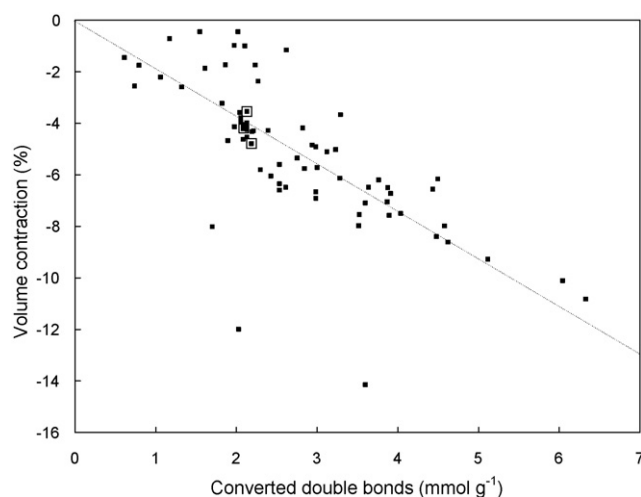


**Fig. 1.** Plot of the volume contraction versus absolute double bond conversion for a wide range of radiation-cured acrylate resins. For instance, the two outlying data points at  $\approx -12$  and  $-14\%$  shrinkage stand for trimethylolpropane triacrylate (TMPTA) and hexanediol diacrylate (HDDA), respectively. The magnified data points show the L, M and H systems of this study. The line serves as a guide to the eye and results from a linear fit to the full dataset (forced through the origin).

which in turn reflects the heterogeneous character of the material at a molecular scale.

Table 4 shows the concentration of (meth)acrylic double bonds in the liquid resin. The higher amount for the H-formulation results from the difference in reactive diluent with the other systems. It is also noticed that the final double bond conversion of the cured coating decreases with increasing  $T_g$ , presumably as a consequence of the reduction of the polymerization rate in the glassy region.

As shown later, the magnitude of the residual stress after photopolymerization can be estimated from the volume contraction. Fig. 1 shows a plot of the volume contraction as a function of the actual double bond conversion for a large number of free-standing acrylate films, either prepared by electron-beam or ultraviolet radiation curing.<sup>3</sup> The magnified points represent the three coatings of this study. The actual double bond conversion was calculated from the initial amount of meth(acrylic) double bonds in the liquid resin and the average conversion rate. The experimental errors are better than 10% for both axes. The scattered data reveal a linear trend but the correlation is poor. Upon polymerization, double bond conversion will result in chemical shrinkage but part of the double bonds will also contribute to gel formation and/or vitrification which explains why a trend emerges. The degree of conversion alone is not sufficient to account for the overall volume contraction,

<sup>3</sup> It is emphasized that the polymerization reactions occurred in non-isothermal conditions.

**Table 4**  
Properties of the liquid formulations and the UV-cured free-standing clearcoats.

Formulation	Liquid resin		Free-standing clearcoats					
	$N_{db}$ (mmol g <sup>-1</sup> )	$\rho_\ell$ (g mL <sup>-1</sup> )	Double bond conversion (%)	$\rho_s$ (g mL <sup>-1</sup> )	Volume contraction (%)	$T_g$ ( $\Delta T_g$ ) (°C)	$E'_0$ (MPa)	$SF_{MEK}$ (%)
L	1.92	1.117	>95	1.158	-3.5	15 (37)	1.5	33
M	1.95	1.100	>90	1.148	-4.2	34 (50)	2.3	27
H	2.17	1.094	≈90	1.149	-4.8	66 (69)	12	15

structural factors should be considered as well. Vitrification, either thermally induced or reaction induced, gives rise to a dramatical loss of configurational entropy and a reduction of specific volume which depends strongly on molecular structure and functionality. Reaction- or cure-induced vitrification but also gel formation should be understood in terms of free-volume or entropy theories which have been introduced originally to account for the reduction of the specific volume upon cooling [13,14].

The storage modulus in the high temperature plateau,  $E'_0$ , is proportional to the density of elastically effective network strands, often referred to as crosslink density. Monoacrylate diluents do not form chemical crosslinks upon polymerization but essentially contribute to chain extension. This is the case for the L and M formulations where the chemical crosslinks of the cured network mainly result from the urethane acrylate oligomer. In contrast, the triacrylate diluent OTA480 will effectively increase the network density upon curing. In the assumption that four crosslinks are created upon reaction of the three double bonds of a single OTA480 molecule, an increase of the crosslink density by a factor of 5.7 is roughly estimated for the H-system as compared to the M-system (M and H share the same oligomer UA2). This is in good agreement with the increase of  $E'_0$  by a factor 5.2 as reported in Table 4. The network density of M is about 1.5 times higher than that of the L-system.

Solvent swelling is very sensitive to the network density but also to the interaction between coating and solvent which makes it less prone for interpretation. Yet, an effect of crosslink density is invoked here to account for the lower swelling factor of the H-system.

The ultimate tensile properties and Young's modulus of the three coating systems are summarized in Table 5. Typical stress-strain curves measured at room temperature are shown in Fig. 2 and behave as expected from the respective  $T_g$  of the coating, i.e., the L system is a soft material (low Young's modulus) with a weak strength, the M coating is stronger with a better resistance to fracture and the H coating is quite hard revealing some ductile behaviour but still with early failure. From a practical point of view, flexibility is often understood as the resistance to fracture upon bending. Accordingly, it is then predicted that M and L are more flexible than H which is in agreement with the T-bend and impact test results. It is noticed, however, that confusion may arise when flexibility is defined in terms of the bending stiffness which characterizes the resistance of a coating towards bending under a given load. Recall that the bending stiffness is proportional to Young's modulus but also to the third power of the thickness! At a fixed thickness, it can be stated that the flexibility of the coating will

**Table 5**  
Average tensile properties of the UV-cured free-standing films.

Clearcoat	$E_Y$ (MPa)	Ultimate tensile strength (MPa)	Elongation at break (%)
L	1.9	1.0	67
M	25	6.0	95
H	254	12	25

decrease by a factor ten from L to M and another tenfold from M to H, according to Young's modulus in Table 5.

Finally, the level of volume contraction provides an indication for the development of stress in the coating upon curing. Stress can lead to defects (e.g., buckling, curling, cracking, delamination) that degrade the final coating quality [15–19]. Most coatings prepared from a liquid develop stress as the liquid transforms into an elastic or viscoelastic solid. Since the coating adheres to a rigid substrate (galvanised steel), shrinkage can occur only into the thickness direction. The constrained volume change in direction parallel to the substrate leads to in-plane tensile stress. As long as the viscous state prevails, the material will be able to relax the stress. However, when the coating solidifies (roughly about the point where  $T_g$  of the curing coating reaches the reaction temperature), internal stress will develop. By multiplying the volume contraction and Young's modulus, an upper bound for the stress can be provided and is 0.07, 1.0, and 12 MPa for L, M and H, respectively. Stress levels of a few MPa and more are relatively high and become critical with regard to adhesion performances.

Evidently, thermodynamic adhesion forces at the interface should be considered as well in order to assess the adhesion strength. From the contact angle data, the estimated surface free energy of the UV-cured L, M and H coating were respectively  $\gamma_C \approx 54, 47$  and  $51 \text{ mJ m}^{-2}$ . For the cleaned HDG panel, a value  $\gamma_S \approx 38 \text{ mJ m}^{-2}$  was found. The thermodynamic work of adhesion,  $W_a$ , is then calculated using the equation-of-state approach, i.e.,

$$W_a = 2\sqrt{\gamma_C \gamma_S} e^{-\beta(\gamma_C - \gamma_S)^2}$$

where  $\beta = 1.25 \times 10^{-4} \text{ m}^2 \text{ mJ}^{-1}$  is an empirical constant. The interfacial work of adhesion of the L, M and H coating with respect

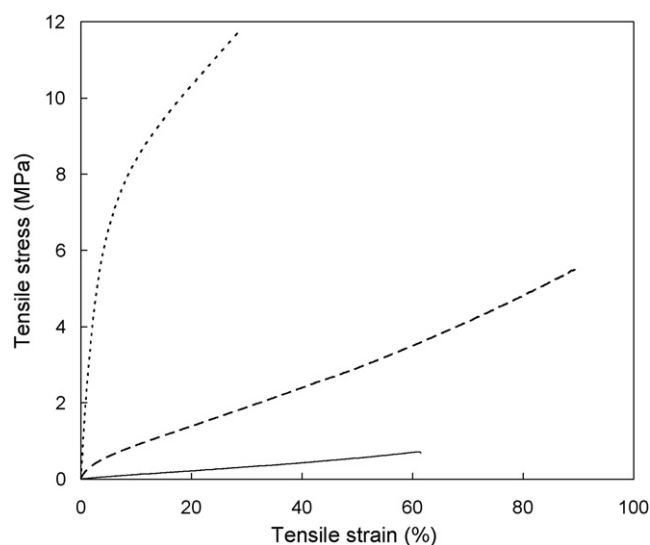


**Fig. 2.** Tensile properties for UV-cured free-standing films L, M and H resins (full, dashed and dotted line, respectively).

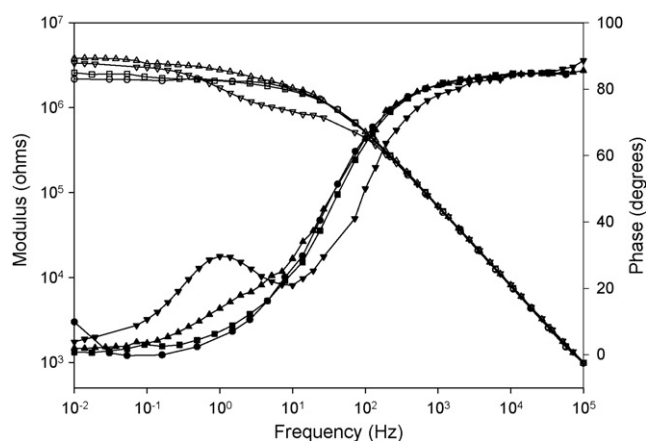


**Fig. 3.** Bode data of the M20 sample after 2 h (circles), 1 day (squares), 3 days (triangles) and 7 days (inverted triangles) of exposure. The open and solid symbols refer to the modulus and the phase shift of the impedance, respectively.

to the cleaned HDG substrate is 88, 84 and 87 mJm<sup>-2</sup>, respectively. The values are not significantly different and this suggests that the overall adhesion strength will primarily be affected by the level of internal stress. Within the accuracy of the data, this is largely verified from the adhesion performances in Table 3.

### 3.3. Electrochemical impedance measurements

#### 3.3.1. Barrier properties

The corrosion resistance of the three clearcoats applied on galvanised steel was evaluated by means of electrochemical impedance spectroscopy. The data are shown according to the Bode representation (impedance modulus and phase shift).

The barrier properties of the different UV-coating systems can be discussed in terms of the low frequency impedance modulus ( $|Z|_{0.01 \text{ Hz}}$ ) which corresponds to the sum of the different resistances offered by the system, including pore and polarisation resistance. The changes of  $|Z|_{0.01 \text{ Hz}}$  are mainly due to the decrease of the pore resistance and to the loss of the barrier properties of the film. When corrosion phenomena occur, a second time constant appears at low frequency and can be detected in the phase shift plots.

As an example, the Bode plots for the M20 sample are shown in Fig. 3 as a function of immersion time in the electrolyte solution. As expected for this kind of relatively simple and non-optimized coating, the electrochemical behaviour is not purely capacitive even for short exposure times. At low frequencies (<10 Hz) a resistive plateau is observed whereas a capacitive behaviour is evidenced in the high frequency range. After an exposure time of 1 day, only one time constant characteristic of the clearcoat system is detected. After 3 days, however, a second time constant appears at low frequencies ( $\approx 1 \text{ Hz}$ ) being a feature of the interface corrosion reaction. Along with the second time constant evidenced in the phase shift curves, a second resistive step becomes apparent in the modulus curve after 7 days of exposure.

These curves illustrate that the low frequency modulus stays quite constant with respect to the exposure time in the electrolyte. In order to compare the three coating systems, the Bode plots obtained after an exposure time of 3 days are shown in Fig. 4 for the L20, M20 and H20 samples. It appears that the barrier properties of the different systems are nearly the same. However, the appearance of a second time constant in the phase shift curve clearly suggests that the H system provides the lowest protection. In contrast, the L

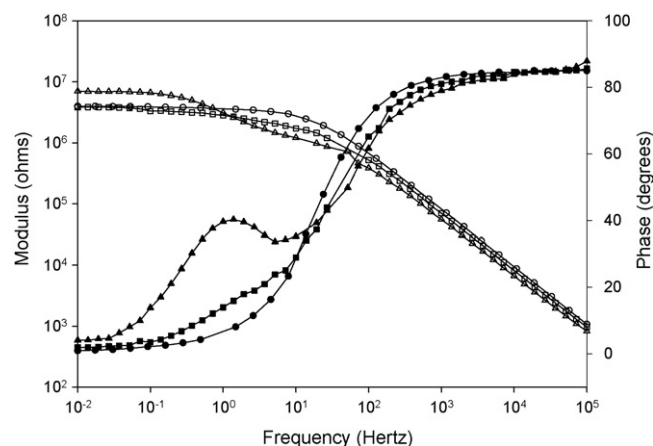


**Fig. 4.** Comparison of the Bode data after 3 days of exposure for L20 (circles), M20 (squares) and H20 (triangles) samples. The open and solid symbols refer to the modulus and the phase shift of the impedance, respectively.

system exhibits a single time constant showing that no significant corrosion phenomena occurred after 3 days. The M system exhibits an intermediate behaviour.

#### 3.3.2. Water permeability

The water permeability of the UV-cured coatings was evaluated by calculating the coating capacitance,  $C_C$  (in Fcm<sup>-2</sup>), at a fixed frequency (10<sup>4</sup> Hz) for an exposed area of 7 cm<sup>2</sup> using

$$C_C = \frac{1}{7\omega |Z|}$$

where  $|Z|$  is the impedance modulus and  $\omega = 2\pi\nu$  is the angular frequency. As shown in Figs. 3 and 4, the behaviour is purely capacitive at 10<sup>4</sup> Hz and the capacitance corresponds to the dielectric behaviour of the coating. The coating capacitance is generally assumed to be a measure of water absorption by the coating and is defined as

$$C_C = \frac{\epsilon_C \epsilon_0 A}{d}$$

where  $\epsilon_C$  is the dielectric constant of the coating,  $\epsilon_0$  is the permittivity of the vacuum,  $A$  is the area of the coating and  $d$  is its thickness. As the dielectric constant of water is about twenty times the value for a typical coating, water penetration will usually lead to an increase of the coating capacitance.

Fig. 5 shows the evolution of  $C_C$  for the L, M and H systems at a target thickness of 20  $\mu\text{m}$ . The  $C_C$  values are relatively constant during the first day of exposure and we can conclude that no significant water uptake occurs in these coatings. Nevertheless, the L system exhibits a small increase of  $C_C$  within the first 6 h which reveals some water absorption, possibly as a consequence of the low  $T_g$  of the coating. As shown before, this weak water uptake (less than 2%) does not affect the barrier properties of the coating. It is noticed that the difference in  $C_C$  between the three systems is primarily related to a variation in coating thickness.

#### 3.3.3. Influence of the coating thickness

The influence of the film thickness on the barrier properties was studied for the three systems. For this purpose, the low frequency impedance modulus was analysed as it reflects the protective properties for the overall system. In Fig. 6, the evolution of  $|Z|_{0.01 \text{ Hz}}$  after 1 day of exposure is examined as a function of coating thickness. An increase of  $|Z|_{0.01 \text{ Hz}}$  with coating thickness is clearly evidenced

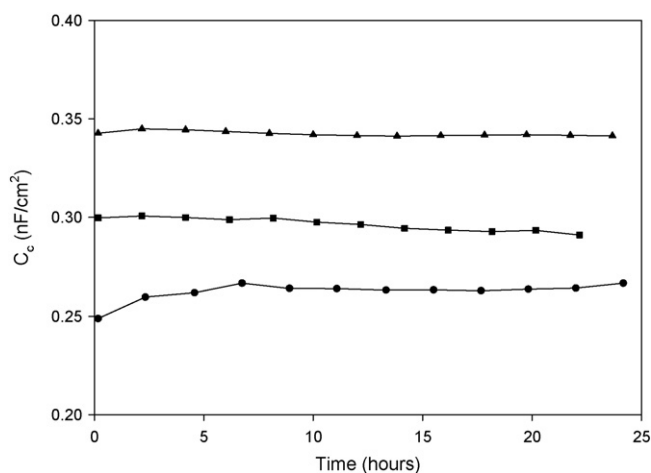


Fig. 5. Time evolution of the coating capacitance for the L20 (circles), M20 (squares) and H20 (triangles) samples.

for the L and M systems. This was not observed for the H system due to its high sensitivity to corrosion. Indeed, a second time constant appears in the Bode plots within the first day of exposure, irrespective of the coating thickness. The H coating layer is porous and systematically exhibits defects preventing the improvement of the barrier properties with increasing thickness. As previously mentioned, the L system offers the best protection with the highest values for the low frequency modulus over the investigated thickness range.

Finally, the volume fraction of absorbed water,  $X_V$ , was calculated from the coating capacitance at  $10^4$  Hz using the Brasher–Kingsbury equation [7,20],

$$X_V = \frac{\log C_t / C_0}{\log \varepsilon_w}$$

where  $C_t$  is the capacitance at time  $t$ ,  $C_0$  is the dry film capacitance and  $\varepsilon_w = 80$  is the dielectric constant of water at room temperature. Fig. 7 provides a plot of the water uptake after 1 day of exposure as a function of the coating thickness. As previously mentioned, the water uptake for the 20  $\mu\text{m}$  coatings is very weak (less than 2% for L system and nearly zero for the two other systems). For thicker coatings, however, an increase of the water absorption is

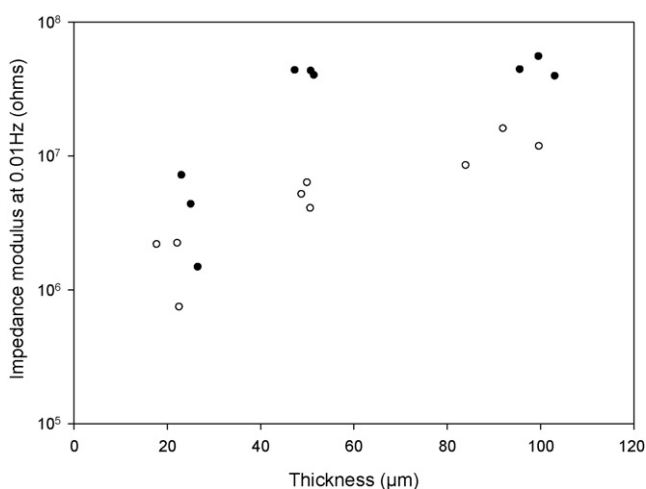


Fig. 6. Plot of the low frequency impedance modulus,  $|Z|_{0.01 \text{ Hz}}$ , as a function of the coating thickness after 1 day of exposure for the L and M system (solid and open symbols, respectively).

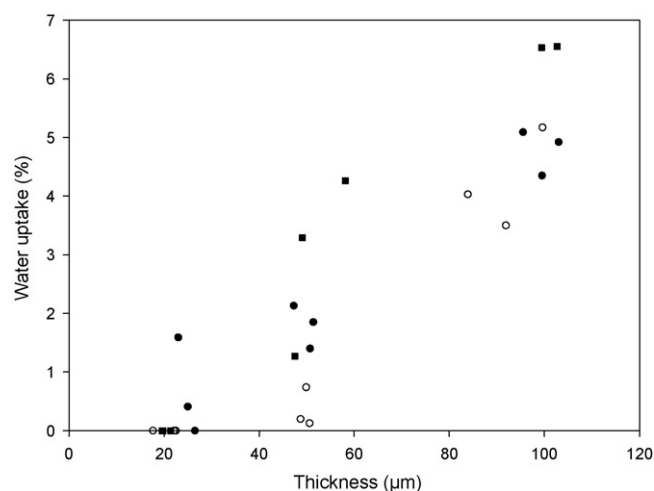


Fig. 7. Water uptake after 1 day of exposure as a function of coating thickness for the L (solid circles), M (open circles) and H system (squares).

noticed which is likely explained by a reduction of the crosslinking efficiency of the UV-curing process with increasing thickness [19].

#### 4. Conclusion

This study achieves a double goal. On the one hand, it highlights that a specific design of radiation curable oligomers with a specific choice of monomers (and other formulation constituents for systems more complex than those investigated here) allows meeting the stringent technical requirements of the metal industry. It demonstrates definitely that the radiation curing technology offers attractive perspectives for metal coatings. On the other hand, this paper reports a first attempt to find correlations between the practical performance tests of the metal industry (cross-hatch adhesion, T-bend, salt spray, etc.) and finer physico-chemical characteristics of the coatings such as tensile, shrinkage and barrier properties. The study of the three fairly simple formulations already shows some interesting trends and opens the door for further product design.

#### Acknowledgements

I.F. and P.R. wish to thank L. Brewaeyns, M.-C. Coulon, R. Gremmel-prez, A. Herssens, E. Jeuniaux, Th. Lardot, G. Lepage and S. Vrijssen for their help in synthesis, sample preparation, application and analysis. Th. Randoux is acknowledged for a critical review of the paper.

#### References

- [1] K. Buysens, M. Tielemans, Th. Randoux, Surf. Coat. Int. A 86 (2003) 179.
- [2] M. Heylen, Proceedings of the RadTech Europe Conference, Barcelona, vol. 1, 2005, p. 179.
- [3] G. Bierwagen, D. Tallman, J. Li, L. He, C. Jeffcoate, Prog. Org. Coat. 46 (2003) 148.
- [4] F. Mansfeld, J. Appl. Electrochem. 25 (1995) 187.
- [5] A. Amirudin, D. Thierry, Prog. Org. Coat. 26 (1995) 1.
- [6] F. Deflorian, L. Fedrizzi, J. Adhes. Sci. Technol. 13 (1999) 629.
- [7] U. Rammelt, G. Reinhard, Prog. Org. Coat. 21 (1992) 205.
- [8] D.Y. Kwok, A.W. Neumann, Adv. Colloid Interface Sci. 81 (1999) 167.
- [9] H. Tavana, A.W. Neumann, Adv. Colloid Interface Sci. 132 (2007) 1.
- [10] P.R. Chalker, S.J. Bull, D.S. Rickerby, Mater. Sci. Eng. A140 (1991) 583.
- [11] S.G. Croll, J. Coat. Tech. 52 (1980) 35.
- [12] Ph. Barbeau, J.F. Gerard, B. Magny, J.P. Pascault, G. Vigier, J. Polym. Sci., Part B: Polym. Phys. 37 (1999) 919.
- [13] L.H. Sperling, Introduction to Physical Polymer Science, J. Wiley & Sons, New York, 1986.

- [14] R.G. Larson, *The Structure and Rheology of Complex Fluids*, Oxford University Press, New York, 1999.
- [15] J.A. Payne, L.F. Francis, A.V. McCormick, *J. Appl. Polym. Sci.* 66 (1997) 1267.
- [16] L.F. Francis, A.V. McCormick, D.M. Vaessen, J.A. Payne, *J. Mater. Sci.* 37 (2002) 4717.
- [17] H. Lu, J.F. Stansbury, C.N. Bowman, *Dental Mater.* 20 (2004) 979.
- [18] A.A. Stolov, T. Xie, J. Penelle, S.L. Hsu, *Macromolecules* 33 (2000) 6970.
- [19] A.A. Stolov, T. Xie, J. Penelle, S.L. Hsu, *Macromolecules* 34 (2001) 2865.
- [20] D.M. Brasher, A.H. Kingsbury, *J. Appl. Chem.* 4 (1954) 62.